

OmegaCam H α segmented filter tests

Review/analysis of lab appraisal carried out June-July 2009

Report: J E Drew, Lab measurements: R Greimel

Summary: The 4-segment H α filter procured by the VPHAS+ consortium was thoroughly tested on receipt in June 2009, measuring the bandpass at 84 positions across the filter mosaic. It was manufactured to a specification of central wavelength, 658.8 nm, and a FWHM band-width of 10.7 nm. A few optical defects were identified then, that demanded some touch up work with black paint – since carried out. Retesting in April 2011 (described in a separate shorter report) indicates that the filter transmission was unchanged after almost 2 years in store, auguring well for its stability over the coming period. Because of the technical difficulty with absolute reproducibility in coating narrowband filters, the 4 segments of the filter are, unsurprisingly, non identical. However, emulation of r-H α , r-i main sequence tracks has shown that the position-dependent throughput variations are close to spectral-type independent across all four filter segments, except for mid/late M dwarfs (not a VPHAS+ science driver). This means that corrections can be applied, provided the necessary calibration data are acquired – namely, good quality accompanying twilight sky flats, specifying to 0.01 magnitude accuracy (or better) the bandpass-integrated throughput variation with position across the filter. A mapping of this kind should be capable of correcting for magnitude variations of around 0.05 that are otherwise predicted to be present. This mapping will be required in any event, in order to characterise vignetting due to the T bars holding the filter segments in place. Simulations of emission line spectra have also been undertaken, which confirm the corners of segment D (the most redshifted) as the most problematic areas of the filter. However the results, overall, indicate that the filter should reliably distinguish Galactic disk emission line objects in among the overwhelming majority of normal stars, according to expectation.

Procurement and validation history:

An order was placed in 2006 for a 4-segment H α OmegaCam filter with Barr Associates, based on a specification supplied by the OmegaCam consortium. The central wavelength for this filter was specified as 658.8 nm, with a bandpass of 10.7 nm – this admits H α and [NII] 6584, with the slight redshift also suiting the filter to nearby galaxy work. At the time of commissioning the work, the cost of a single-piece narrowband filter was prohibitive – with only one enterprise even willing to consider taking on the job at a price beyond the purchasing consortium’s reach. This restriction on options for procurement remains in place today. Production of the filter was delayed by around 3 years, due to a backlog of work at Barr and – when production did begin – there were further delays while trial and error brought the fabrication to within the specification. Folded into this last period of waiting were issues with filter response to thermal cycling, prompted in part by unexpected breakages of other filters delivered to the OmegaCam consortium.

Measurements were performed immediately on the receipt of the 4-segment H α filter, by Robert Greimel. They were carried out at the University of Munich Observatory, using the optical lab set up by the OmegaCam consortium for all such characterisation exercises: each segment was measured across a grid of 21 positions (see figure below), using a monochromator beam adjusted to emulate the beam geometry of VST/OmegaCam. What these tests do not emulate is the true effect of vignetting due to the pair of T bars holding the segments in place, or the larger spot size at the filter plane, mounted in the telescope, associated with point sources brought to a focus in the camera

image plane. The impact of these factors will have to be evaluated on sky.

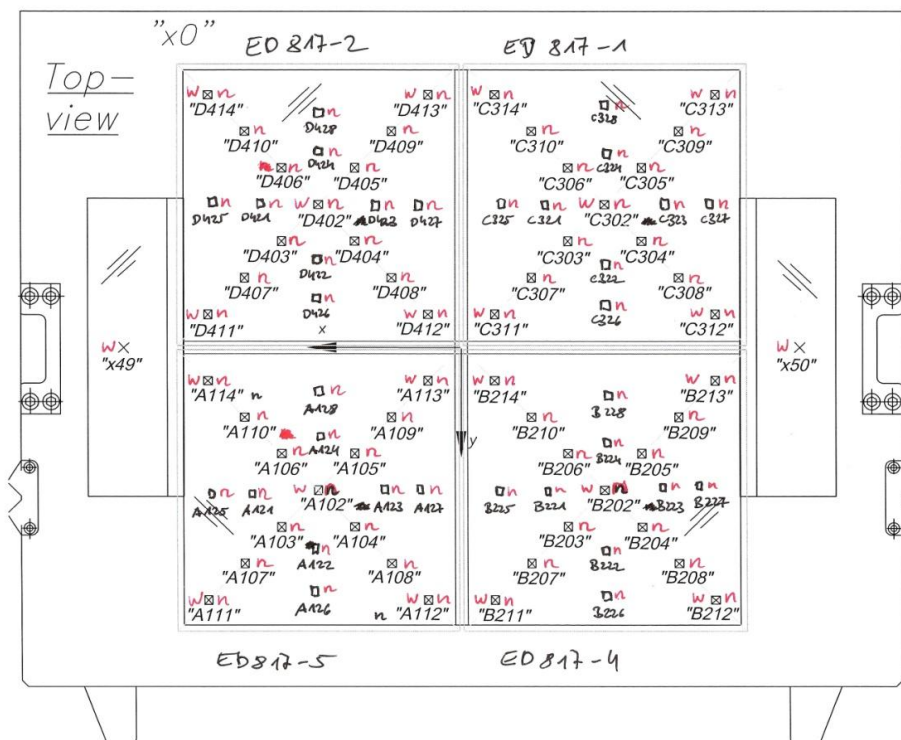


Figure 1: Plan of the filter mosaic, showing the naming scheme for the segments and the locations where the transmission profile was measured. In each segment there are 21 positions.

The tests performed revealed that one of the 4 segments (segment D) did not meet with the specification on central-wavelength shifts across its entire area, and there were concerns at the time about cosmetic quality. For these two reasons the consortium pursued possible remedies with Barr (who subsequently changed ownership twice) but, in the end, no changes were possible. It remains

the case that the far corners of segment D diverge most from the mean in representing the variation of r-H α colour with spectral type – altogether, this kind of issue should not affect more than a few percent of all eventually catalogued data . The worst of the cosmetic issues – a couple of nicks in the surface of segment B – have since been dealt with by Jean-Louis Lizon, who applied matt black paint to them to prevent the potential introduction of continuum light into the $\sim 10\text{nm}$ band-pass. Fixes of this kind are not unusual. We are extremely grateful to Jean-Louis for his steady hand and nerves in taking this on.

When the filter was inspected and the necessary paintwork discussed with Jean-Louis in September 2010, it was noticed there might be the beginnings of some blooming on segment B. It was to check this that retesting was undertaken in April 2011 by Bill Martin. The conclusion from this was that the filter has been stable, and that the possible hint of blooming is in fact an area of solvent staining or similar that had not been cleaned off (i.e. a cosmetic problem). The transmission tests do not indicate a noticeable impact of this staining on throughput. At this point it was concluded the filter was ready for on-sky tests as we had exhausted what could reasonably be done in the lab.

Below we present the detail of the direct results of visual inspection, the measurements and main-sequence track emulation based on the measurements.

Visual inspection:

On receipt of the mosaic, it was noticed by Bernard Muschielok and Robert Greimel that the filter had a number of cosmetic imperfections, the worst of which were in segment B. Some had already been noted to us by Barr, e.g. in the auxiliary guide panels, where they had attempted some of their

own black-paint remedy. Hand-drawn sketches were made to record them for later correction.

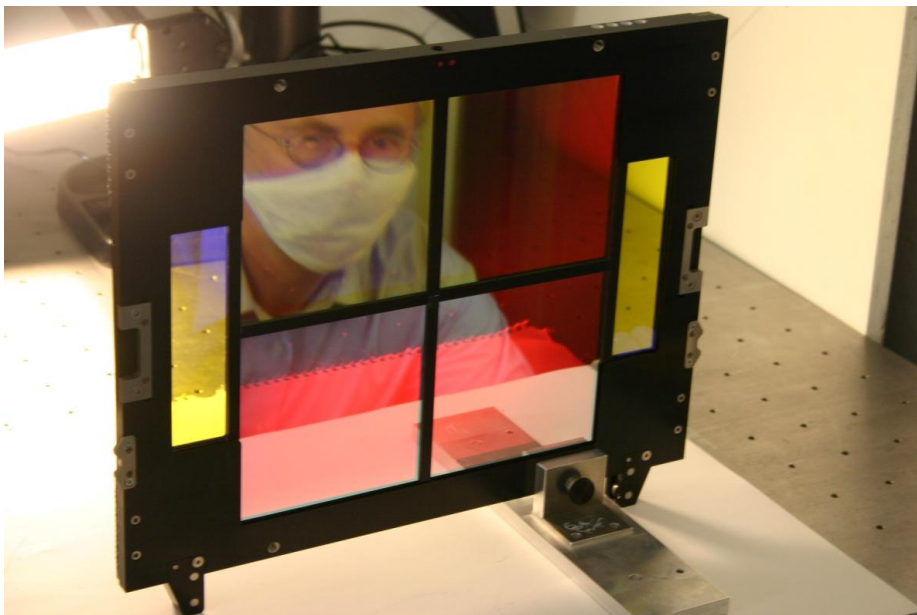


Figure 2: photo of the filter taken 22/6/2009 in Munich at the start of the lab evaluation.

Measurements:

These are made using a monochromator beam size of 4-5 mm. In comparison, at the telescope, starlight will occupy a spotsize of diameter of up to 12 mm on passing through the filter. Hence the actual performance will be a smoothed version of what is revealed by these measurements and their subsequent simulation.

The main summarising data derived from the transmission-curve measurements for the 13 positions forming the two diagonals in each segment are listed in the table below. In each line the column entries are:

File-name (encoding date/time, position, wedge setting code); peak transmission; transmission FWHM (nm); central wavelength (nm); wavelength shift from nominal (nm); profile integral

Table 1:-

Segment A

090622_1616_Halpha-partAn_#A102__44	0.973	10.121	658.015	-0.785	10.079
090622_1902_Halpha-partAn_#A103__47	0.958	10.202	657.867	-0.933	9.664
090624_1802_Halpha-partAn_#A104__45	0.964	10.183	658.026	-0.774	9.988
090624_2051_Halpha-partAn_#A105__43	0.963	10.222	658.142	-0.658	10.026
090624_1821_Halpha-partAn_#A106__45	0.958	10.196	658.010	-0.790	9.970
090623_2154_Halpha-partAn_#A107__48	0.951	10.268	658.119	-0.681	9.869
090624_2320_Halpha-partAn_#A108__46	0.962	10.157	658.530	-0.270	9.923
090623_2252_Halpha-partAn_#A109__42	0.965	10.279	658.728	-0.072	10.105
090624_2302_Halpha-partAn_#A110__46	0.949	10.275	658.374	-0.426	9.864
090623_1339_Halpha-partAn_#A111__49	0.943	10.090	659.051	+0.251	9.459
090622_1924_Halpha-partAn_#A112__47	0.960	10.030	659.641	+0.841	9.607
090623_1029_Halpha-partAn_#A113__41	0.953	10.141	659.990	+1.190	9.802
090622_1944_Halpha-partAn_#A114__47	0.947	10.159	659.436	+0.636	9.555

Segment B:

090623_1005_Halpha-partBn_#B202__44	0.972	10.379	659.614	+0.814	10.273
090624_1840_Halpha-partBn_#B203__45	0.979	10.385	659.207	+0.407	10.384
090623_0816_Halpha-partBn_#B204__47	0.974	10.339	659.104	+0.304	10.271
090624_1858_Halpha-partBn_#B205__45	0.974	10.337	659.314	+0.514	10.236
090624_2110_Halpha-partBn_#B206__43	0.976	10.423	659.373	+0.573	10.345
090625_0800_Halpha-partBn_#B207__46	0.976	10.410	658.331	-0.469	10.413
090623_2213_Halpha-partBn_#B208__48	0.978	10.363	658.218	-0.582	10.341
090625_0819_Halpha-partBn_#B209__46	0.979	10.331	658.463	-0.337	10.254
090624_0903_Halpha-partBn_#B210__42	0.977	10.625	658.419	-0.381	10.475

090623_0857_Halpha-partBn_#B211__47	0.971	10.461	657.953	-0.847	10.359
090623_1235_Halpha-partBn_#B212__49	0.975	10.370	657.902	-0.898	10.296
090622_2047_Halpha-partBn_#B213__47	0.971	10.446	657.940	-0.860	10.272
090623_1139_Halpha-partBn_#B214__41	0.973	10.934	657.782	-1.018	10.575

Segment C:

090623_0944_Halpha-partCn_#C302__44	0.963	10.031	658.288	-0.512	9.869
090624_2128_Halpha-partCn_#C303__43	0.971	10.058	658.642	-0.158	9.987
090624_1918_Halpha-partCn_#C304__45	0.968	10.031	658.562	-0.238	9.935
090623_0755_Halpha-partCn_#C305__47	0.966	10.014	658.490	-0.310	9.903
090624_1936_Halpha-partCn_#C306__45	0.972	10.008	658.610	-0.190	9.946
090624_0844_Halpha-partCn_#C307__42	0.972	10.254	659.406	+0.606	10.146
090624_2148_Halpha-partCn_#C308__46	0.968	10.129	659.304	+0.504	9.953
090623_2232_Halpha-partCn_#C309__48	0.974	10.092	659.113	+0.313	9.963
090624_2206_Halpha-partCn_#C310__46	0.968	10.106	659.288	+0.488	9.950
090623_1119_Halpha-partCn_#C311__41	0.970	10.345	660.172	+1.372	10.168
090622_2127_Halpha-partCn_#C312__47	0.973	10.116	659.992	+1.192	9.966
090623_1256_Halpha-partCn_#C313__49	0.966	10.083	659.758	+0.958	9.874
090622_2147_Halpha-partCn_#C314__47	0.968	10.121	659.995	+1.195	9.962

Segment D:

090622_1837_Halpha-partDn_#D402__44	0.968	10.107	658.174	-0.626	10.002
090624_1955_Halpha-partDn_#D403__45	0.968	10.084	658.451	-0.349	9.986
090624_2033_Halpha-partDn_#D404__43	0.969	10.122	658.599	-0.201	10.033
090624_2014_Halpha-partDn_#D405__45	0.967	10.104	658.664	-0.136	9.993
090622_2217_Halpha-partDn_#D406__47	0.967	10.105	658.448	-0.352	9.972
090624_2243_Halpha-partDn_#D407__46	0.962	10.175	659.315	+0.515	9.954
090624_0819_Halpha-partDn_#D408__42	0.965	10.294	659.522	+0.722	10.101
090624_2225_Halpha-partDn_#D409__46	0.966	10.198	659.490	+0.690	9.965
090623_2135_Halpha-partDn_#D410__48	0.967	10.209	659.252	+0.452	9.960
090622_2237_Halpha-partDn_#D411__47	0.952	10.157	660.255	+1.455	9.818
090623_1057_Halpha-partDn_#D412__41	0.964	10.382	660.619	+1.819	10.050
090622_2257_Halpha-partDn_#D413__47	0.951	10.132	660.503	+1.703	9.667
090623_1316_Halpha-partDn_#D414__49	0.958	10.143	660.153	+1.353	9.712

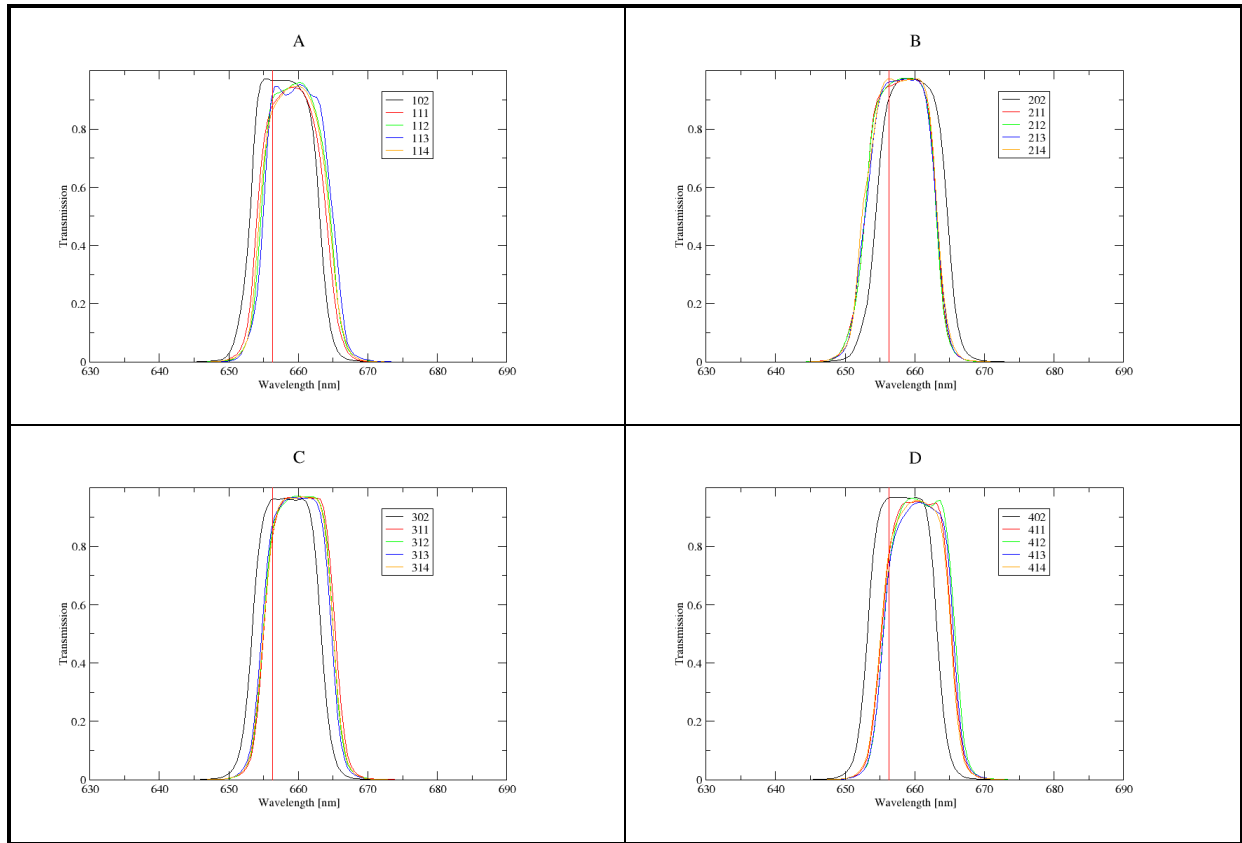


Figure 3: Transmission profiles of segment corners compared with segment centres.

The general pattern for segments A, C and D is for the central wavelength (CWL) to be shortest in the segment centre, becoming progressively longer as the corners are approached (along the diagonals). Strikingly, this pattern is reversed for segment B. Above, the measured transmission curves at the centres and four corners of all segments are shown to bring out this main point of contrast between B and the others. A second way in which this segment stands out is that it presents with the highest mean FWHM, and highest average peak transmission (see discussion, below, of main sequence tracks).

Main sequence track simulations:

The transmission curves were fed into trial simulations of r - $H\alpha$, r - i colour-colour tracks for main sequence stars in order to better understand the band-integrated behaviour of the filter segment. This involves synthetic photometry following the procedures described in the IPHAS survey paper (Drew et al 2005 MNRAS 362 753), in which the transmission curves are folded with a typical CCD response and library flux-calibrated stellar spectra, in order to predict r , i and $H\alpha$ magnitudes that are then combined to produce the colour-colour diagram. The choice of r , i filter transmission curve and/or CCD response is not relevant to this exercise (all taken from the INT/WFC), as the focus is on how the changing spectra of MS stars interact with the varying transmission across the $H\alpha$ filter. A good result here consists of: (a) no/little variation in the vertical position of the MS track in the colour-colour plane as a function of position on filter, (b) no/little variation in the *shape* of the track with filter position. Note that vertical shifts violating (a) can be calibrated out, straightforwardly in principle, while shape changes represent a much tougher challenge.

The behaviours of all 84 measured transmission curves have been simulated in this way, using a common assumed value for the integrated flux of Vega – arbitrarily chosen as its flux obtained on passing through the filter at position D402.

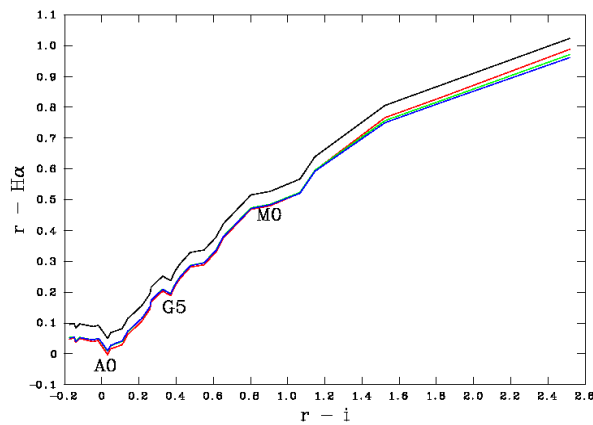


Figure 4: A direct comparison of the mean MS ($r-H\alpha, r-i$) tracks obtained for each segment, showing B (black line, top) admits 4.5 percent more flux than the other 3. The labels A0, G5 and M0 mark the spectral types the intrinsic colours correspond to.

Above, the mean tracks obtained for each segment are compared. The outstanding difference is that segment B is displaced by upwards ~ 0.045 magnitudes, because its greater typical bandwidth combined with slightly superior peak transmission admits more light. Otherwise the tracks follow the same shape up to about $r-i = 1.2$ (corresponding to M3 spectral type), but after that there is some divergence.

The variance in track properties with position across each segment has also been examined in order to appraise how the centre-to-corner gradients in transmission affect them. This exercise reveals that the corners of segment A and D vary noticeably from the mean trend in $r - H\alpha$ colour with $r - i$. Otherwise, there is some range in $r - H\alpha$ offset (~ 0.03 typically) but the colour dependences are similar. This could prove to be correctable via good flat-fielding. Below, the results for all measured positions are presented, as the difference between computed MS track and the segment mean.

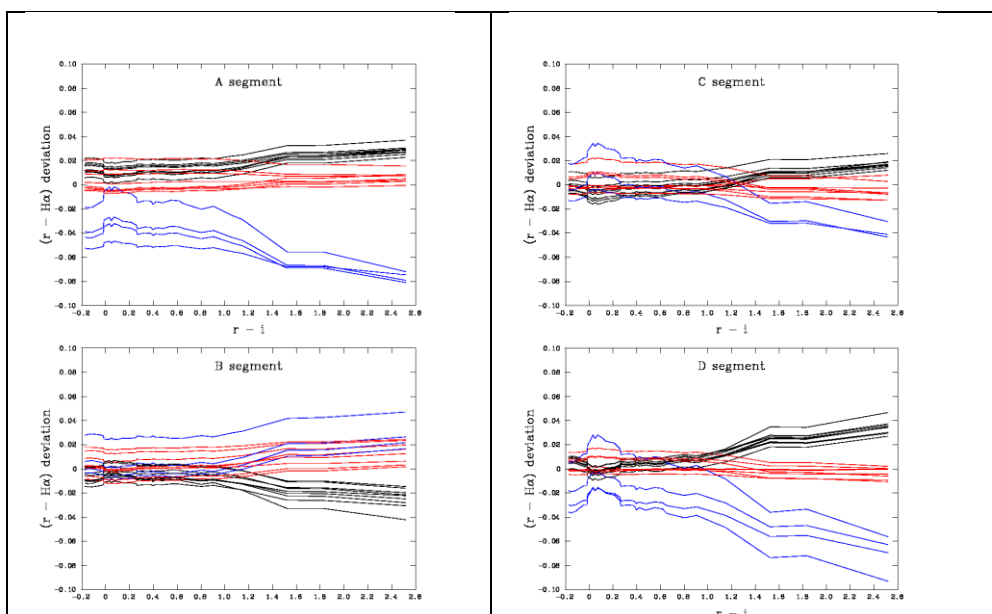


Figure 5: Each curve shown is obtained by subtracting the segment mean MS colour-colour track from each individual simulated track. The curves in black are from around segment centre (positions 2-6, and 21-24), those in red are from the ring of positions around these (positions 7-10, and 25-28), while finally, those in blue are the corner positions (11-14).

these (positions 7-10, and 25-28), while finally, those in blue are the corner positions (11-14).

We put to the test the idea that much of the spread in figure 5 is correctable, if a rescaling is applied that takes out the variations of the integrated throughput. To do this, the throughput data in the final column of table 1 have been taken as the basis for calculating (colour-independent) MS-track offsets in $r - H\alpha$. The reference MS track was constructed by taking the mean of all tracks except those measured for the corners of segments A, C and D and the centre of segment B (where the central wavelength is also somewhat redshifted) – the reference integrated throughput was calculated on the same basis. The resultant curves are shown below.

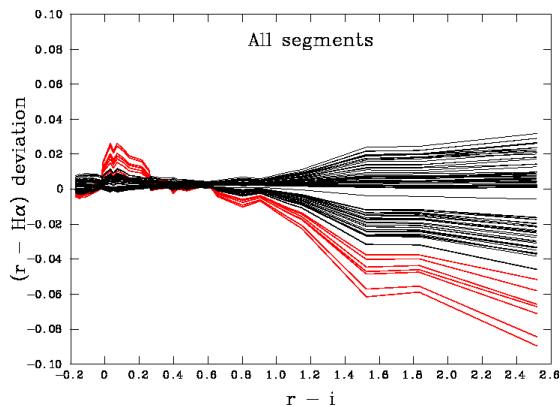


Figure 6. The $r - H\alpha$ deviations computed for all measured positions, after correcting the data for bandpass integrated throughput variations. The data plotted in red are associated with the measurement locations picked out in red (in the CWL shift column) in Table 1 – these locations are: all corners of segment D, three corners in segment C and one in a corner of segment A.

This result also better quantifies the problem that arises with mid-late M stars in that, by $r - i = 1.4$, there is a range in measured/corrected $H\alpha$ magnitude across the filter approaching 0.05 magnitudes, in place of the much tighter dispersion seen at $r - i < 1.0$ (where it is under 0.01). Is this increased dispersion a problem, and can it be circumvented? The figure below provides an example of a northern hemisphere IPHAS colour-colour diagram as evidence that it is unlikely to be more of a problem than it has been in the past: the essential point is that later M dwarfs are sufficiently faint that they normally appear in colour-colour diagrams as a relatively sparse, scarcely reddened local population – rising as a thinly populated spur at $r - H\alpha > 0.6$ (left hand panel below). More reddened dwarfs are often just too faint.

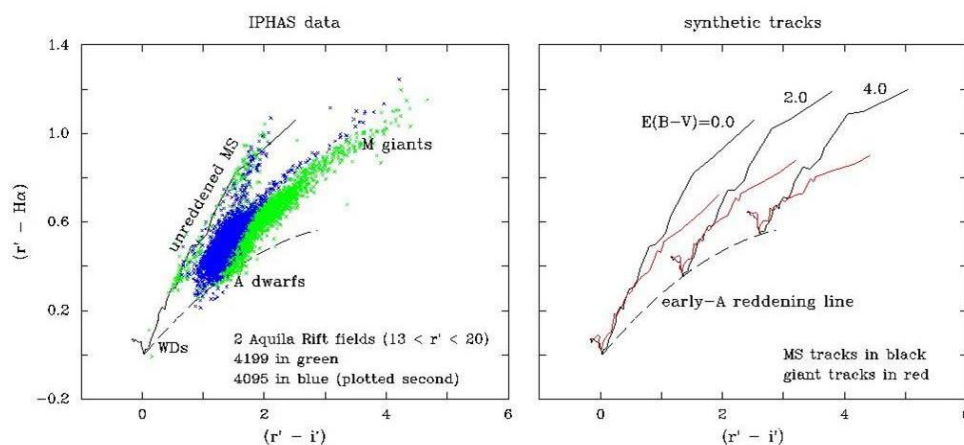


Figure 7: from Drew et al (2005) – a comparison of real colours versus predicted colours.

What has not been tested (simulated) yet is how much blurring will be seen in the M-giant spur at the shallower angle seen in figure 7. However it will be true, regardless of luminosity class, that within limited regions of the filter mosaic of order the size of a single CCD, the filter properties are

not changing so fast that there will be significant sequence blurring. Hence the work-around, if needed to deal with this problem, will be to extract and calibrate more locally.

It is worthy of note that the pattern of behaviour presented in figure undergoes little change as reddening is introduced. This was checked by recalculating tracks for $E(B-V) = 2$, or A_V of order 6 and plotting them as above: the changes noted were small.

Identification and measurement of emission line objects:

Simulations have also been performed to consider how the filter captures $H\alpha$ flux, as function of position/segment. A perfect filter, well-centred on the mean wavelength of $H\alpha$ emission imaged would show no variation in transmitted flux or magnitude, and would not be sensitive to modest velocity shifts. We are looking for facility of separation between $H\alpha$ emission line objects and the main stellar locus – and, ideally, a regular mapping of measured $r - H\alpha$ excess onto emission equivalent width (cf Drew et al 2005, figure 6). The spectra used to explore sensitivity to velocity shifts are shown below.

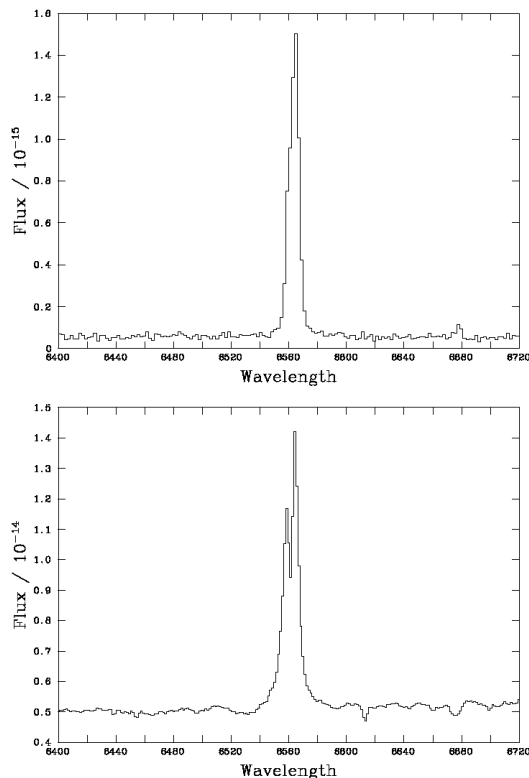


Figure 8. *Top panel:* this is an example of a very bright, simple $H\alpha$ emission profile (from Corradi et al 2010). The EW of emission is ~ 220 Angstrom, and the FWHM of the observed profile is close to 390 km/s. The mean radial velocity of the line is +35 km/s. The difference between a pure continuum magnitude and that including the line is >1.2 , in this case. *Lower panel:* the contrast of the line is much less here (EW ~ 20 Angstrom), and the FWHM is somewhat wider at 570 km/s (from Raddi et al, in prep). The mean radial velocity is -50 km/s. The continuum-only magnitude is fainter by about 0.2 only.

Both spectra were shifted to centre at the wavelength corresponding to -500 km/s, and then shifted redward in steps of 100 km/s at a time, up to $+500$ km/s (altogether a

displacement of 0.22 nm) – calculating at each step the integral of the spectrum folded through the filter transmission profile. The resultant in-band ‘fluxes’ were converted to magnitudes, adopting as the reference the mean flux computed for positions 2-6 and 21-24 for segment A. In real use, we would expect most emission line objects to present with FWHM below that of either of these examples (excepting e.g. interacting binaries and WR stars), and that as mainly thin disk objects they would be centred on radial velocities within the range -150 to $+150$ km/s. The results, as graphs, are below.

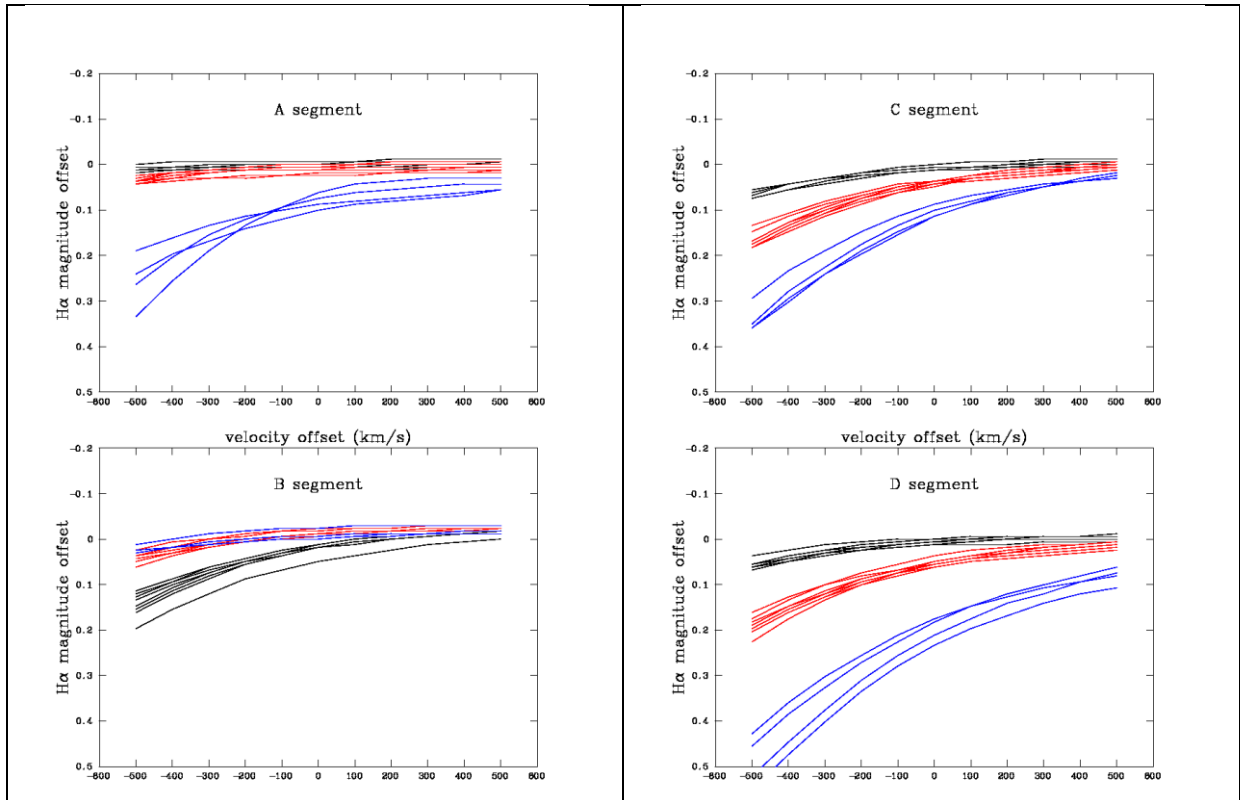


Figure 9: Results for the EW = 220 Angstroms emission spectrum (upper panel figure 8). The curves are colour-coded as before with the corner positions picked out in blue.

The different character of segment B shows up in the slope of response apparent across its centre – attributable to the relative redshift of the transmission profile there. Roles are reversed dramatically in segment D, where the redshift of the transmission in the corners is particularly marked, giving rise to the strong positive gradients seen in the plot above. Segments A and C are ‘in between’ in behaviour. Regardless of where the image of such a star might fall on the filter, the magnitude shifts are never so large that there would ever be a failure to pick the object up as a strong H α emitter. However, the corners in all but segment B would ‘under-predict’ the emission equivalent width. In the corners of D, the shortfall could be in the region of 25 percent. This is unfortunate, but not catastrophic – especially when it is remembered that (i) the VPHAS+ strategy will typically provide a second pointing away from the corners, (ii) variability is notable property of H α emission in many objects.

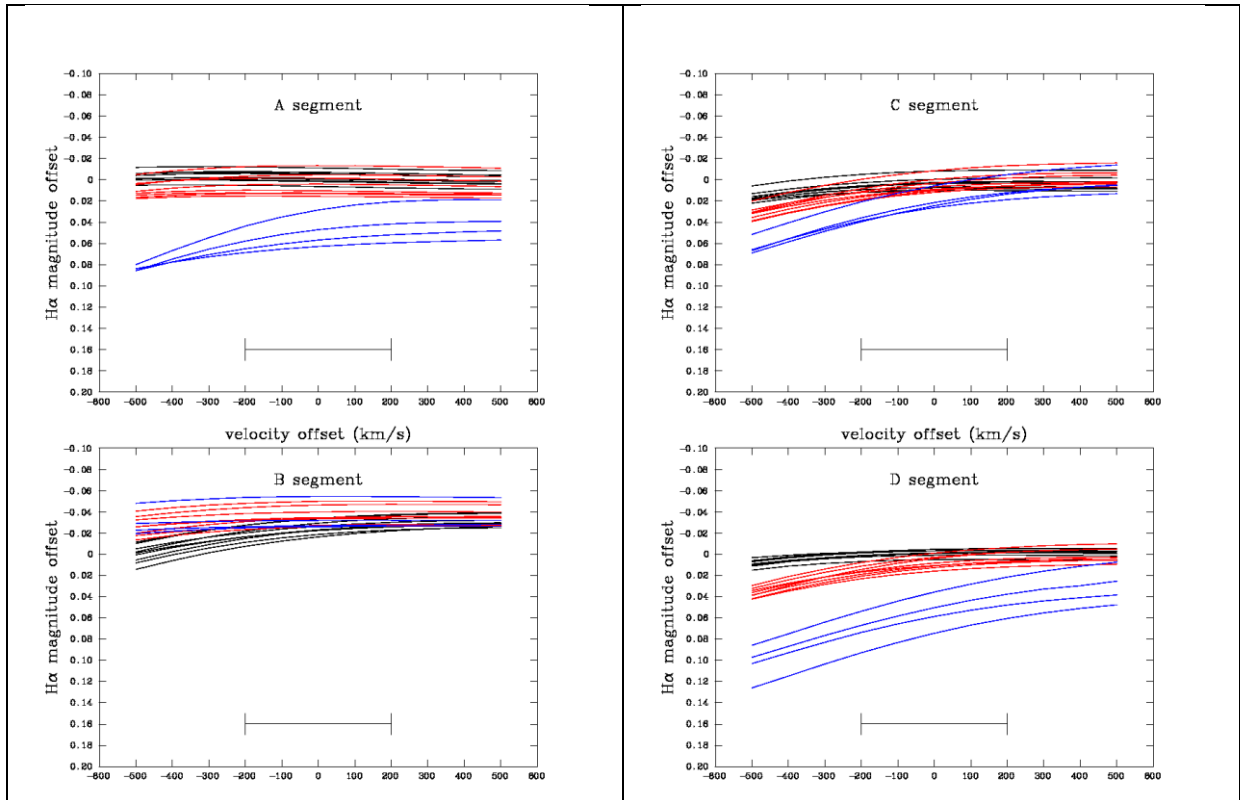


Figure 10. Results for an emission line net equivalent width of 20 Angstroms (spectrum shown in lower panel in figure 8). The bar picks out the radial velocity range most relevant to the Galactic Plane, and it is placed at the magnitude offset that corresponds to the inband flux, in the absence of the excess line emission.

In this case, the line emission itself contributes under 20 percent of the total in-band flux (assuming all the emission is captured). This reduces the magnitude shift seen in the corners of segments D and A. At negligible reddenings, the effects seen here are not large enough to prevent the identification of emission line objects in colour-colour diagrams involving $r - H\alpha$, because the main stellar locus – essentially the unreddened main sequence – may be 0.2 or more magnitudes away (see Drew et al 2005 fig 6). Where there might be a limited problem is at intermediate reddening (A_V approaching 5–6), as the constant EW track crosses into the rising unreddened MS: in effect, some objects will be lost prematurely if imaged *only* in the corners of segments D or A.

In summary, the non-uniformity of central wavelength that is characteristic of this particular filter fabrication is likely to lead to:

- A non-unique response to mid-late M stars within the main stellar locus (figures 5, 6)
- Some quantitative under-prediction of net emission line equivalent for objects/nebulosity imaged toward the corners of segment D (a 25 percent effect), and to a lesser extent towards the corners of segment C and A (a 10 percent effect).

This filter is not suitable for use on environments in which the typical radial velocities encountered are much below -200 km/s. It will perform very well at low near-Universe redshifts up to $1-2000$ km/s. Data-taking in the disk of the Milky Way, as part of the VPHAS+ survey, should deliver the quality envisaged for the survey science case: in particular there are no significant threats to the basic task of emission line object discrimination. Only on-sky testing can reveal how good a correction can be made, in reality, for the known position-dependent throughput variations.

(Supplement Report)

OmegaCam H α Mosaic Filter Test

University Observatory Munich

26-28 April 2011

W Martin

I Ilijevski

Summary

The Barr- supplied OmegaCam H α mosaic filter was tested with the large aperture Optical Test Bench at the University Observatory, Munich. The principal objective was to determine whether the filter mosaic had changed since fabrication in 2009. The filter tiles do not appear to have changed from the original test data to within the precision of the measurements, +/-0.1% in transmission, +/-0.2nm in wavelength. Not every tile was tested at every point but the 'worst' appearing, 'B', was examined at four points along the diagonal from the centre to the most cosmetically challenged corner. No significant difference was found with the original Barr test data.

Optical Test Bench

I Ilijevski replaced a defective power supply and checked the instrument for normal operation before the tests as it had been some months since last used. This specialised instrument is an in-house designed single beam spectrophotometer capable of measuring transmission on optics up to 500x500mm. Great care has been taken with the wavelength selection via a double monochromator which also gives excellent rejection of ghosts and grating orders. The single beam design means that the transmission measurement can, with care, be of the order of +/-0.1%. Measurement statistics were gathered with a bare glass filter and the wavelength calibration was checked with a low pressure Hg lamp. These confirmed that the average one sigma standard deviation for a transmission measurement (five samples) is 0.096% at 90% transmission. Mercury lines were measured to be +/-0.2nm of the accepted value in the range 500-600nm. The wavelength calibration technique is expected to produce similar precision across the 300-1200nm range of the photodiode detector.

The Tests

The mosaic assembly with tiles labelled A-D starting from the lower right corner and going anticlockwise, see Fig 1, was placed in the test enclosure and positioned with fixed spacers at the points indicated. The incidence angle was set with wedges to 1.78-3.14 degrees appropriate for the in-camera beam at each segment position. Each segment was measured at the centre and in the lower right corner. Tile 'B' had a visual appearance that was different from the other three with a 'grainy' appearance and a variation in colour from the centre to the lower right corner. This variation was subtle but easily seen. Small variations between the tiles would indicate that four separate coating operations were needed to produce the array. Transmission measurements were made at wavelengths 638nm to 678nm with a step size of 0.5nm on all the indicated points in Fig 1.

In addition a transmission measurement from 300-1200nm with a resolution of 3nm was performed at position B202 to check blocking performance.

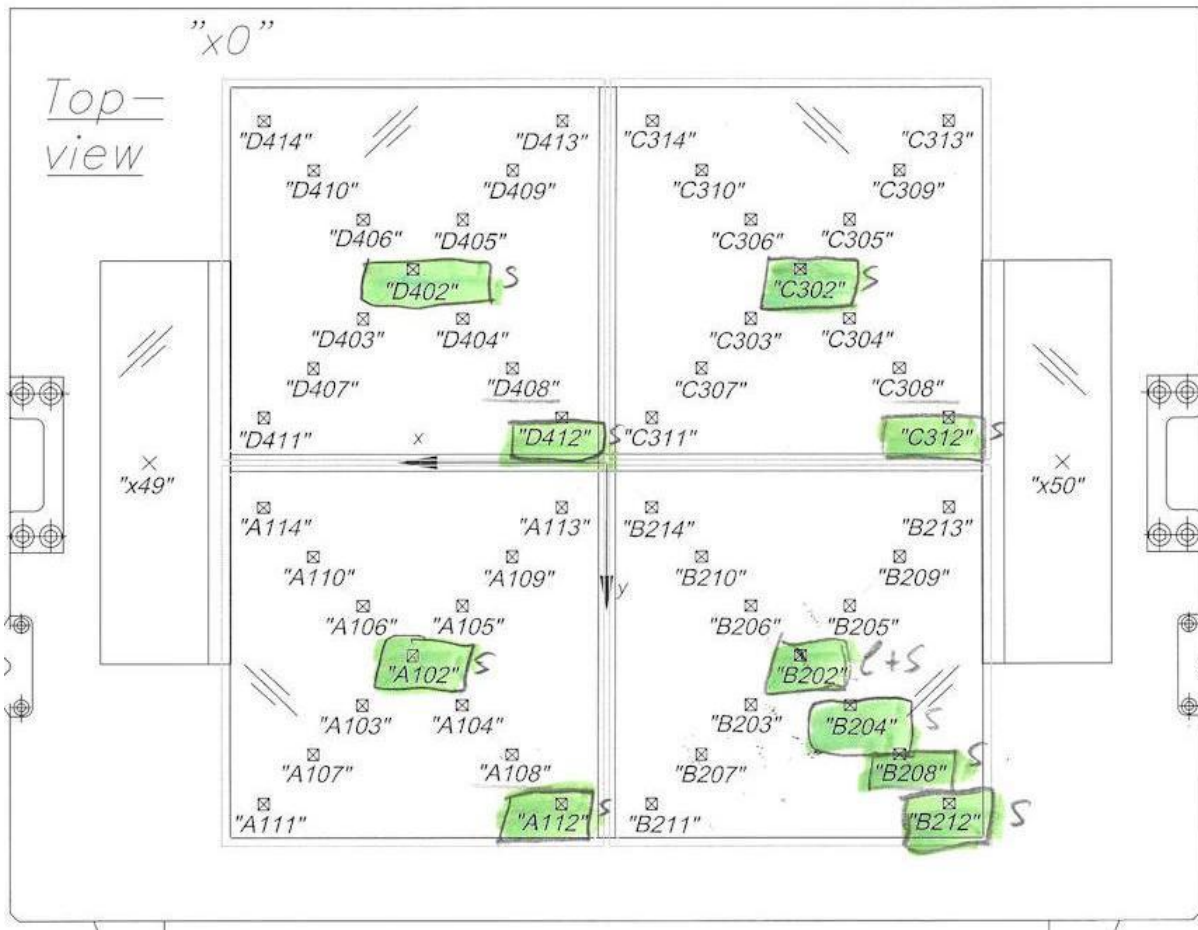


Figure 1. Test locations with respect to the filter mounting frame.

The Results

The three tiles A,C,D had similar transmission curves with the centre wavelength of the pass band shifting $\sim 1\text{nm}$ to a longer wavelength from centre to the corner. Tile 'B' is seen to have a $\sim 1\text{nm}$ shift to a shorter pass band centre wavelength. Fig 2 shows the measurement on each tile centre. Fig 3 shows the measurements at the tile corners. Fig 4 shows the four points B202, B204, B208, B212 along the diagonal of this tile. Fig 5 shows the transmission at point B202 over the range 300-1200nm with the measurements from 645-663nm limited to $6.2\text{e-}4$.

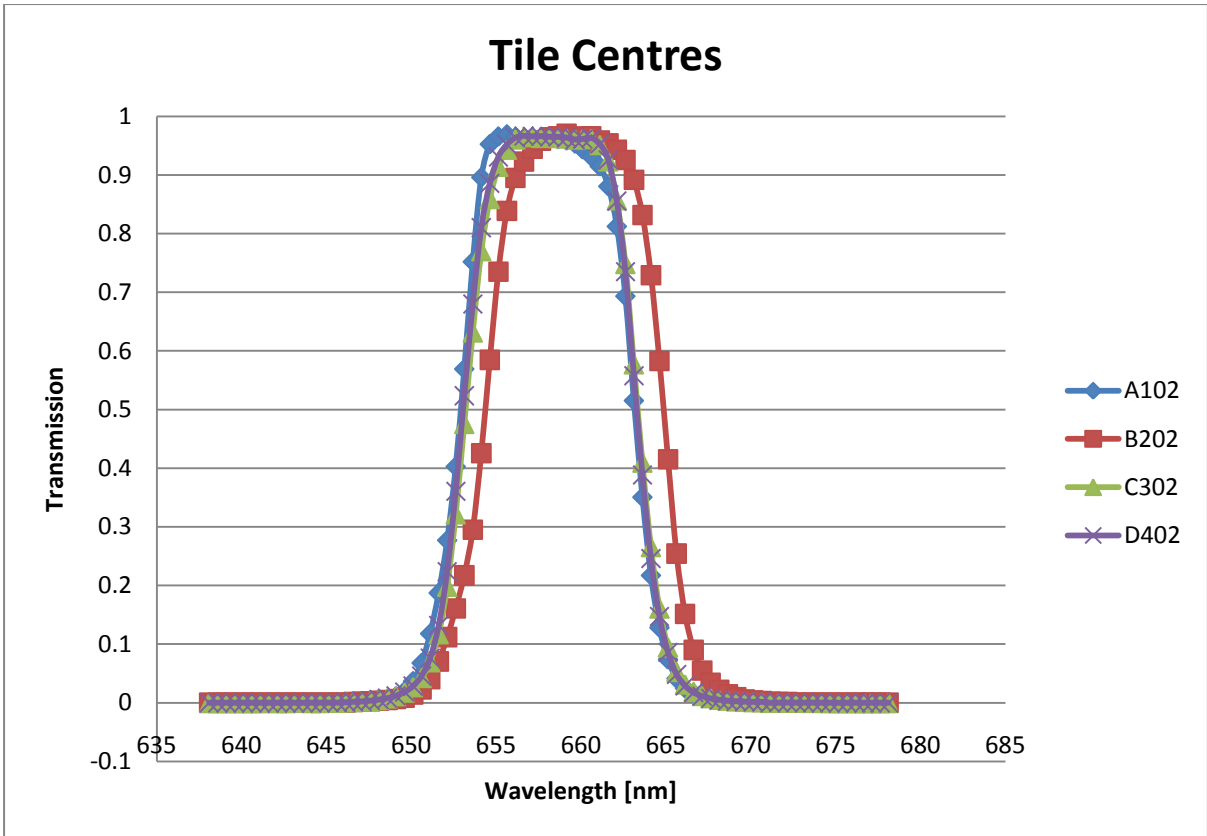


Figure 2. Tile centre band pass transmission.

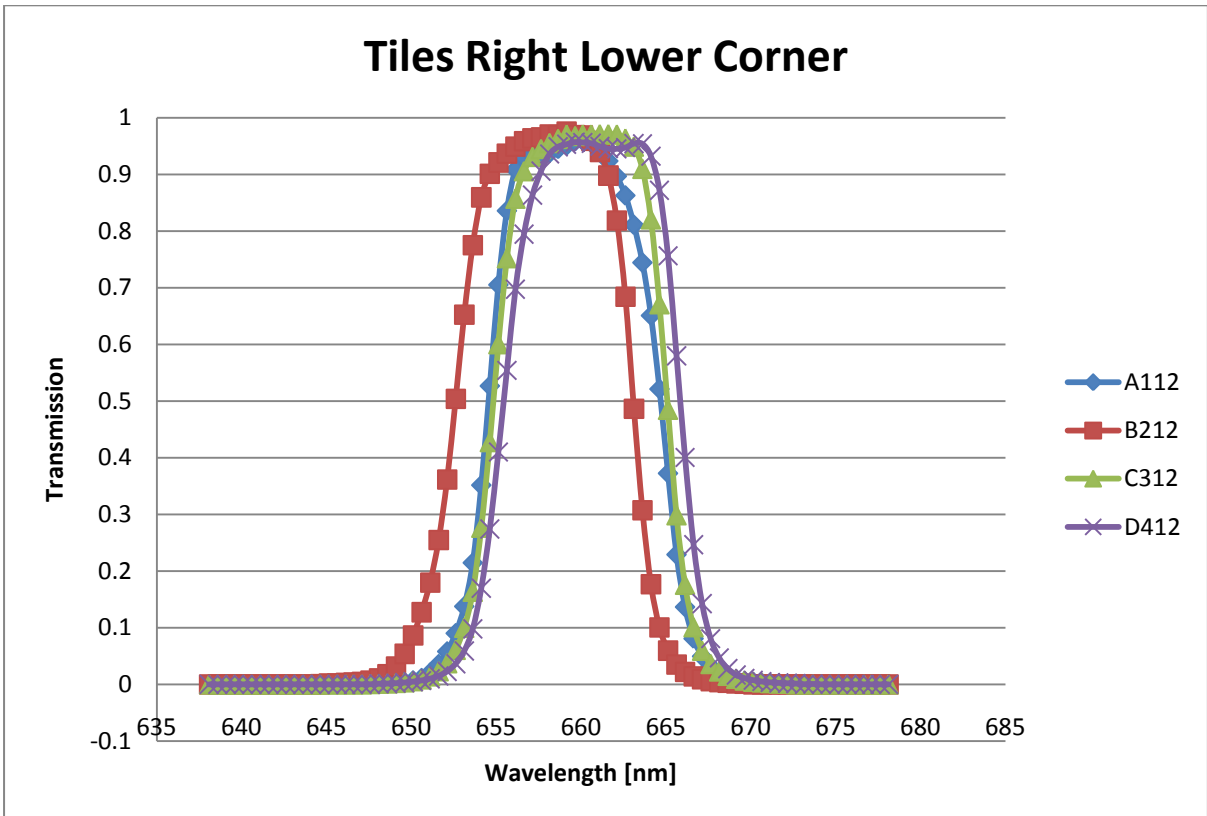


Figure 3. Tile corner bandpass transmission.

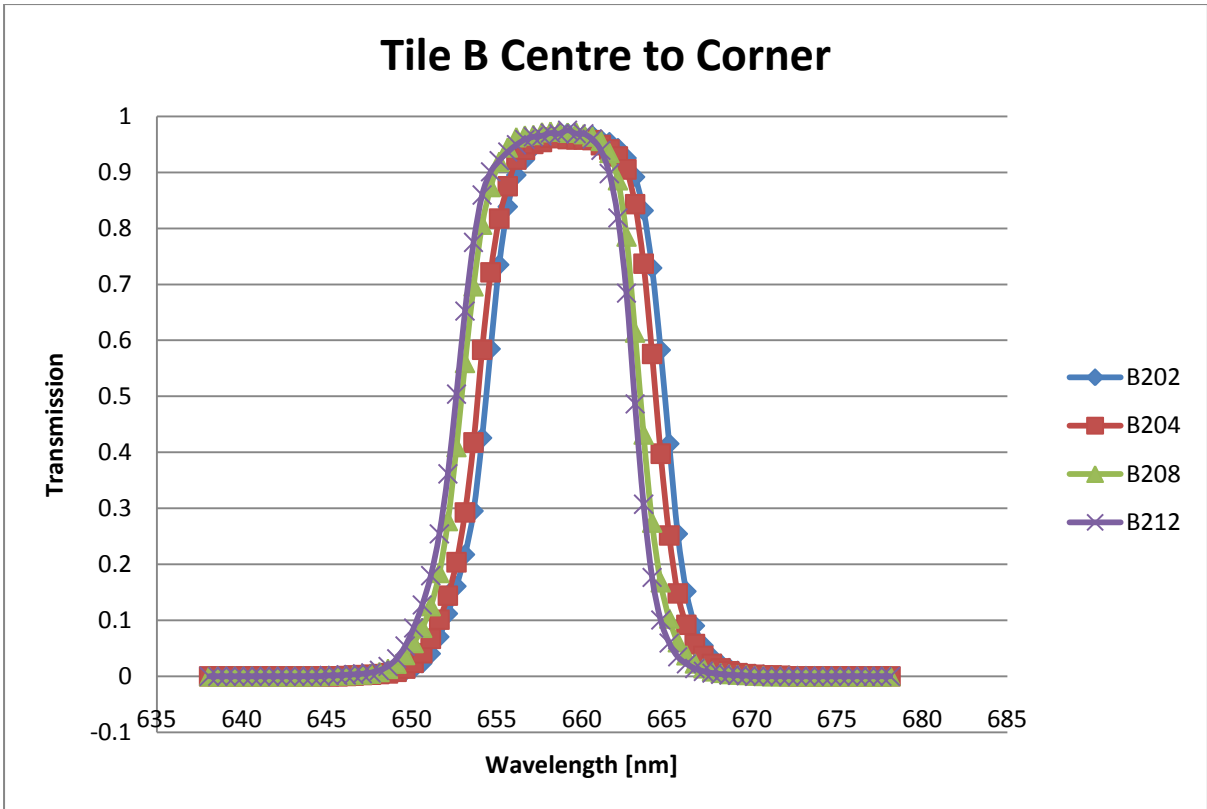


Figure 4. Tile 'B' centre to corner bandpass transmission.

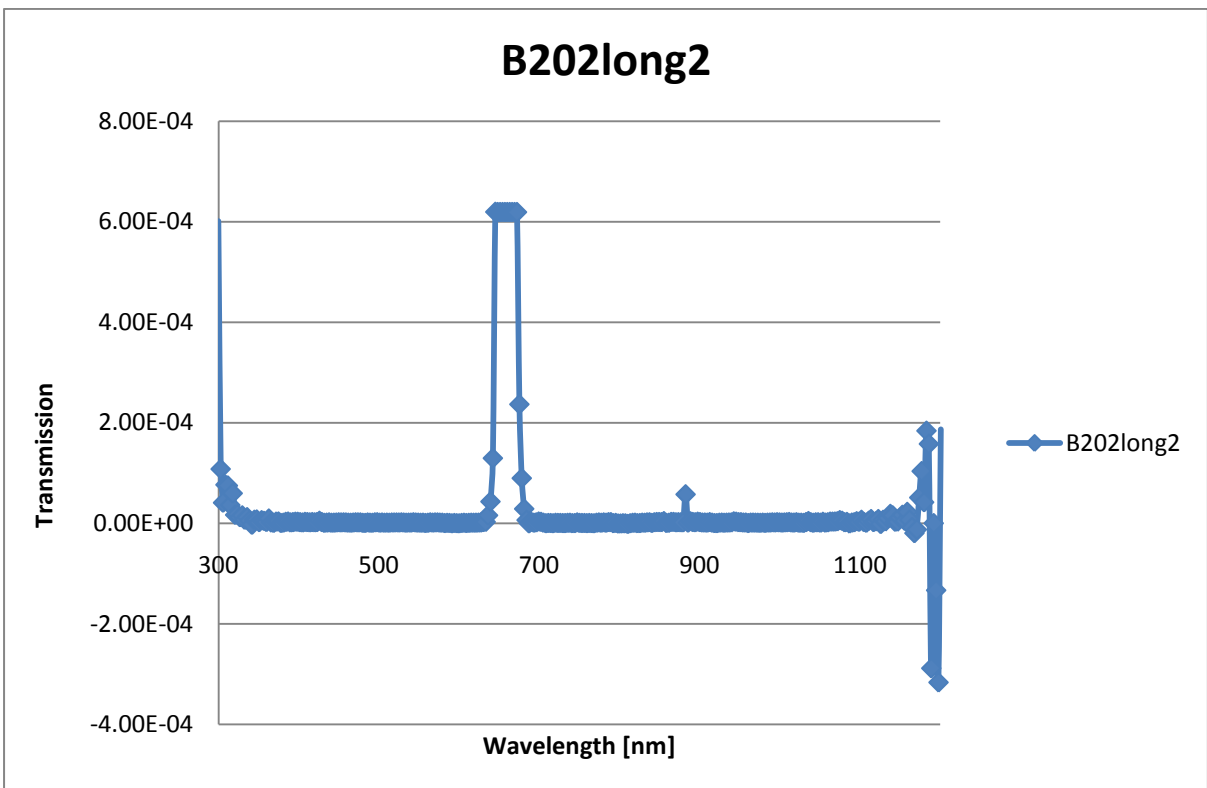


Figure 5. Full spectrum transmission at the centre of tile 'B'. Transmission limited 645-663nm.

Comparison With Barr Test Data

The following graph Fig. 5 shows the Barr test data from 2009 and the current measurements overlaid for tile 'B'. Other tiles show the same relationship new to old, i.e. the transmission measurements agreed to within the precision of the Optical Test Bench limits of $\pm 0.1\%$ and $\pm 0.2\text{nm}$.

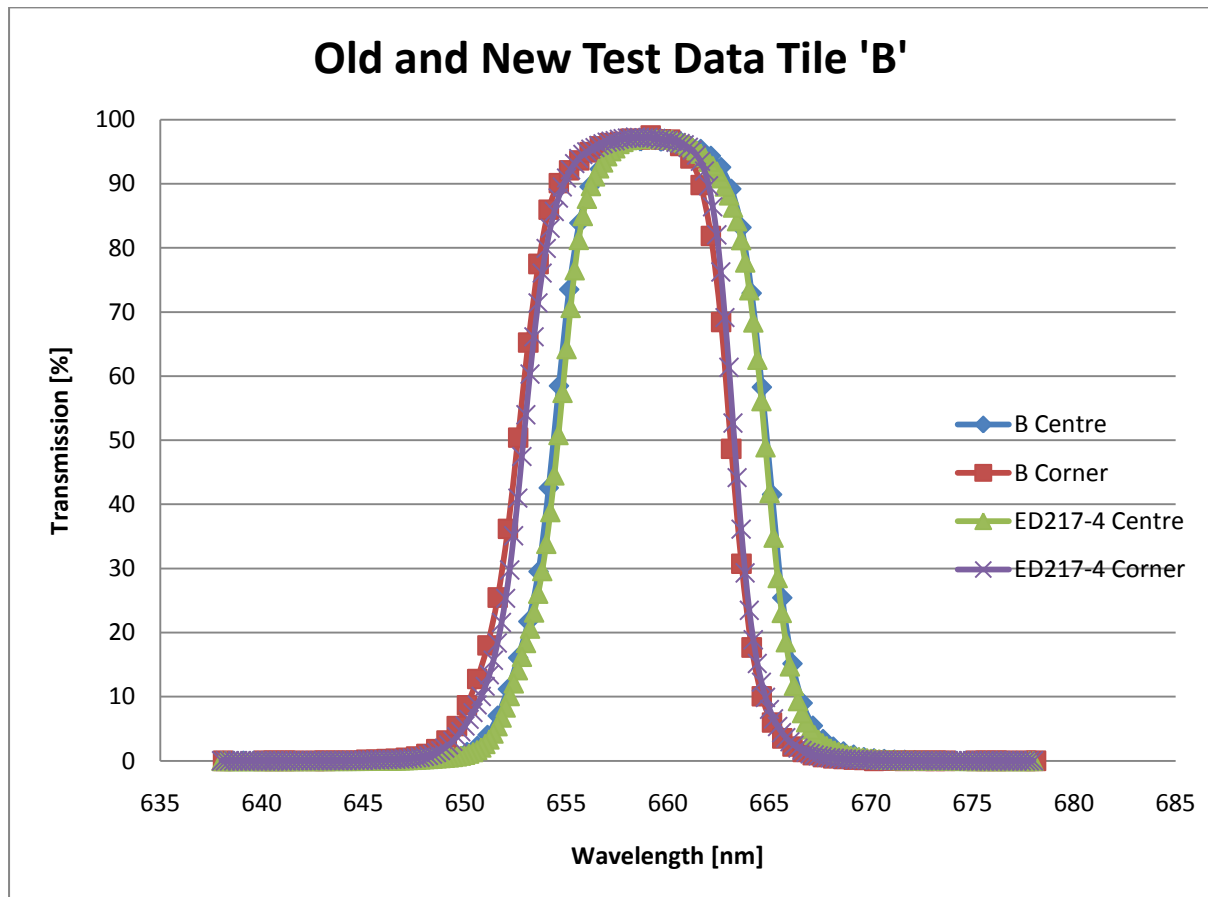


Figure 5. Barr test data (2009) and current measurements.

Conclusions

The test data show that no significant changes have taken place in the filter tiles to within the precision of the measurements of $\pm 0.1\%$ in transmission and $\pm 0.2\text{nm}$ in wavelength. Tile 'B' is the odd one out with a different visible appearance and a centre to corner wavelength shift which is the opposite of the other three tiles. The very different behaviour of tile 'B' will make for some challenges in the photometric reduction of data and the variation in wavelength shifts with position in the overall mosaic will be very difficult to correct for, entirely, in a spectral analysis. The original test data produced by Barr clearly shows the effect. The worst case in the current test data is shown in Figure 3 which has a 2.5nm centre wavelength shift between tile 'B' and tile 'D' at their respective corner positions giving this variation between the centre and edge of the camera FOV. The nominal bandwidths are constant at 10-11nm in all cases (see also curves in first report).

The detailed test data is available in a spreadsheet for additional analysis.

This mosaic of filters, each different and with individual parameters that vary with position will present calibration challenges. The data analysis effort could be substantial if the goal is a photometric calibration driven down to the same precisions as may well be achievable via the unsegmented Sloan filters used in the survey. However, the analysis based on the first more comprehensive set of measurements does indicate that the stated VPHAS+ survey goals of calibration to 0.02—0.03 magnitudes are reachable, if the appropriate calibration data are available.

The specification for a monolithic filter, if sought, should include limits on band shift with respect to azimuthal and radial position – these should be achievable with current large aperture coating technology.